Neuron, Vol. 38, 375–387, May 8, 2003, Copyright ©2003 by Cell Press

Serine 776 of Ataxin-1 Is Critical for Polyglutamine-Induced Disease in *SCA1* Transgenic Mice

Effat S. Emamian,[1,2,4,5] Michael D. Kaytor,[1,2,4] Lisa A. Duvick,[1,2] Tao Zu,[1,2] Susan K. Tousey,[1,2] Huda Y. Zoghbi,[3] H. Brent Clark,[1] and Harry T. Orr[1,2,*]

[1]Department of Laboratory Medicine and Pathology
[2]Institute of Human Genetics
University of Minnesota
Mayo Mail Code 206
Minneapolis, Minnesota 55455
[3]Department of Molecular and Human Genetics
Howard Hughes Medical Institute
Baylor College of Medicine
One Baylor Plaza
Houston, Texas 77030

Summary

Polyglutamine-induced neurodegeneration in transgenic mice carrying the spinocerebellar ataxia type 1 (SCA1) gene is modulated by subcellular distribution of ataxin-1 and by components of the protein folding/degradation machinery. Since phosphorylation is a prominent mechanism by which these processes are regulated, we examined phosphorylation of ataxin-1 and found that serine 776 (S776) was phosphorylated. Residue 776 appeared to affect cellular deposition of ataxin-1[82Q] in that ataxin-1[82Q]-A776 failed to form nuclear inclusions in tissue culture cells. The importance of S776 for polyglutamine-induced pathogenesis was examined by generating ataxin-1[82Q]-A776 transgenic mice. These mice expressed ataxin-1[82Q]-A776 within Purkinje cell nuclei, yet the ability of ataxin-1[82Q]-A776 to induce disease was substantially reduced. These studies demonstrate that polyglutamine tract expansion and localization of ataxin-1 to the nucleus of Purkinje cells are not sufficient to induce disease. We suggest that S776 of ataxin-1 also has a critical role in SCA1 pathogenesis.

Introduction

An intriguing group of human neurodegenerative diseases are those associated with the expansion of a CAG trinucleotide repeat that encodes a glutamine tract within the disease-causing protein (Zoghbi and Orr, 2000; Nakamura et al., 2001). This group of disorders currently includes spinobulbar muscular atrophy (SBMA), Huntington's disease (HD), dentatorubral pallidoluysian atrophy (DRPLA), and the spinocerebellar ataxias (SCA) types 1, 2, 3, 6, 7, and 17. In most of these disorders, a pathological hallmark is the presence of subcellular sites of elevated polyglutamine protein concentration. Often these accumulations appear in the nucleus of neurons and are hence termed intranuclear inclusions. However, for some of these proteins, the accumulations occur in the cytoplasm and/or membrane, as in the cases of SCA2 and SCA6, respectively (Huynh et al., 1999; Ishikawa et al., 1999). The findings that these accumulated proteins redistribute cellular chaperones and components of the ubiquitin proteasome pathway led to the hypothesis that the expanded glutamine tract might cause the host protein to adopt a conformation that may resist degradation and/or affect its interactions with other proteins, leading to downstream toxic effects (Cummings et al., 1998; Chai et al., 1999; Stenoien et al., 1999). Although length of the polyglutamine tract is the major determinant of age of onset and in some instances disease severity, it becomes increasingly clear that neuronal vulnerability and disease progression are not solely dependent on length of the expanded polyglutamine tract. The many observations that an expanded polyglutamine peptide isolated from the intact protein is much more toxic than when in the host protein argues that sequences outside of the glutamine tract function to dampen the deleterious effects of the expanded polyglutamine tract (Wellington and Hayden, 2000; Zoghbi and Botas, 2002). A critical role for sequences outside of the glutamine tract in disease pathogenesis has also been suggested from the point that each disease is characterized by the loss of a specific subset of neurons (Orr, 2001). For example, in SCA1, cerebellar Purkinje cells are a prominent site of pathology (Genis et al., 1995; Robitaille et al., 1995), and in SBMA, it is the spinal motor neurons that are lost (Kennedy et al., 1968). In addition, within the SCAs, a mutant repeat size that causes a juvenile form of SCA1 results in an adult onset form of SCA3. Conversely, repeat lengths that cause adult onset SCA1 cause juvenile onset SCA2. This further suggests that elements outside of the polyglutamine tract can influence the course of disease (Zoghbi, 1996), perhaps through their participation in interactions with other proteins.

Toward understanding the processes that modify SCA1 disease progression, several animal models have been established and investigated (Burright et al., 1995; Fernandez-Funez et al., 2000; Watase et al., 2002). Using a model of Purkinje cell disease in *SCA1* transgenic mice, we found that nuclear localization of mutant ataxin-1 is critical for disease to develop (Klement et al., 1998). Further examination of the *SCA1* mice revealed a set of genes whose expression is decreased in Purkinje cells prior to the onset of pathology, highlighting the potential role of transcriptional regulation and/or RNA stability in pathogenesis (Lin et al., 2000). Analyses of *SCA1* mice also indicate that alterations in protein folding and degradation pathways modify disease progression. Absence of the E3 ubiquitin ligase encoded by the *Ube3A* gene enhances pathology in *SCA1* mice (Cummings et al., 1999). On the other hand, overexpression of the inducible form of the molecular chaperone Hsp70 slows disease progression (Cummings et al., 2001). A genetic screen in a *Drosophila* model of SCA1 identified

*Correspondence: harry@lenti.med.umn.edu
[4]These authors contributed equally to this work.
[5]Present address: The Rockefeller University, New York, New York 10021.

several enhancers and suppressors of the SCA1 phenotype (Fernandez-Funez et al., 2000). Among the SCA1 modifiers identified by this screen were genes encoding components of protein folding and clearance pathways, as well as genes involved in transcriptional regulation, RNA binding, and nuclear localization.

Thus, studies utilizing both mouse and fly models point to nuclear import, gene expression, and protein folding and clearance as processes that impact on SCA1 pathogenesis. It is likely that the effects of many of the modifiers would depend on interactions between ataxin-1 and other proteins that might involve residues outside of the polyglutamine tract. Protein phosphorylation is a prominent mechanism by which protein/protein interactions, including those involving nuclear transport and degradation, are regulated (Hunter, 2000). To assess whether phosphorylation has a role in regulating ataxin-1's function and pathogenicity, we examined the phosphorylation status of ataxin-1 and found that the serine at residue 776 (S776) was a site of phosphorylation. Importantly, neuronal dysfunction is dramatically dampened in mice expressing an *SCA1* transgene encoding ataxin-1 with an expanded polyglutamine tract in which S776 was replaced by an alanine. These results, along with those presented in the paper by Chen et al. (2003 [appearing in *Cell*]) indicate that phosphorylation of S776 plays a key role in modulating the ability of mutant ataxin-1 to induce neurodegeneration by regulating its interactions with other cellular proteins.

Results

Ataxin-1 Is Phosphorylated at Serine 776

Examination of the amino acid sequence of ataxin-1 revealed several possible phosphorylation sites (Banfi et al., 1994). To assess whether any of these sites are phosphorylated, immune-purified ataxin-1[30Q] from stably transfected CHO cells was subjected to tryptic digestion followed by HPLC and mass spectrometry. This analysis examined 30% of the ataxin-1 primary sequence and revealed a single phosphoserine-containing peptide spanning residues Arg774 to Arg781 with the site of phosphorylation being the serine at residue 776 (Figure 1A). To confirm that S776 is a site of phosphorylation of ataxin-1 in vivo, S776 was mutated to an alanine. Transfected cells expressing full-length ataxin-1 with a wild-type glutamine tract and an alanine at position 776 (ataxin-1[30Q]-A776) had a 50% reduction in the amount of ^{33}P incorporated compared to cells expressing ataxin-1[30Q] with a serine (ataxin-1[30Q]-S776) (Figure 1B). Similar results were obtained using cells expressing ataxin-1[82Q]-S776 or ataxin-1[82Q]-A776 (Figure 1C).

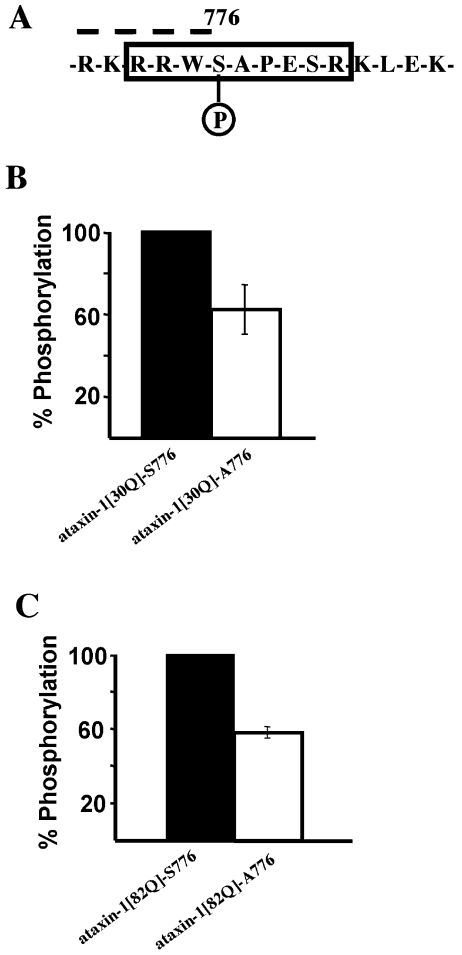

Figure 1. Serine 776 Is a Site of Phosphorylation in Ataxin-1

Numbering of amino acid residues within ataxin-1 is based on a protein with a polyglutamine tract length of 30 residues.

(A) Dashed line depicts the location of the NLS identified previously (Klement et al., 1998). The single phosphopeptide identified by HPLC and mass spectroscopy of ataxin-1[30Q] is designated by the boxed region. Amino acids are indicated using the single letter code.

(B) Percent incorporation of ^{33}P into ataxin-1[30Q]-A776 compared to the incorporation of ^{33}P into ataxin-1[30Q]-S776.

(C) Percent incorporation of ^{33}P into ataxin-1[82Q]-A776 compared to the incorporation of ^{33}P into ataxin-1[82Q]-S776.

Effects of S776 on Nuclear Localization and Solubility of Ataxin-1 in Tissue Culture Cells

cDNA constructs encoding full-length ataxin-1[82Q]-S776 or ataxin-1[82Q]-A776 were used to generate stably expressing ataxin-1 CHO cells. Cells expressing ataxin-1[82Q]-S776 contained large nuclear inclusions as has been typically seen when ataxin-1 is overexpressed in cells (Figure 2A). Surprisingly, few nuclear inclusions were detected in cells overexpressing ataxin-1[82Q]-A776 in spite of its abundant and prominent nuclear localization (Figure 2B). Nuclear inclusions were detected in 60% of the cells expressing ataxin-1[82Q]-S776, while less than 0.1% of the cells expressing ataxin-1[82Q]-A776 contained inclusions (Figure 2C). Thus, S776 in ataxin-1 is not critical for its nuclear localization in transfected cells but clearly plays a major role in its potential to accumulate in nuclear inclusions.

Ataxin-1 with a conformation that seems to resist degradation typically accumulates in these inclusions and is insoluble when extracted. To determine if loss of inclusions in ataxin-1[82Q]-A776 transfected cells affects its conformation and/or solubility, we prepared protein extracts from cells expressing either ataxin-1[82Q]-S776 or ataxin-1[82Q]-A776 and quantified the amount of insoluble ataxin-1. The amount of ataxin-1 in the insoluble fraction decreased drastically (10-fold) from 5% in cells

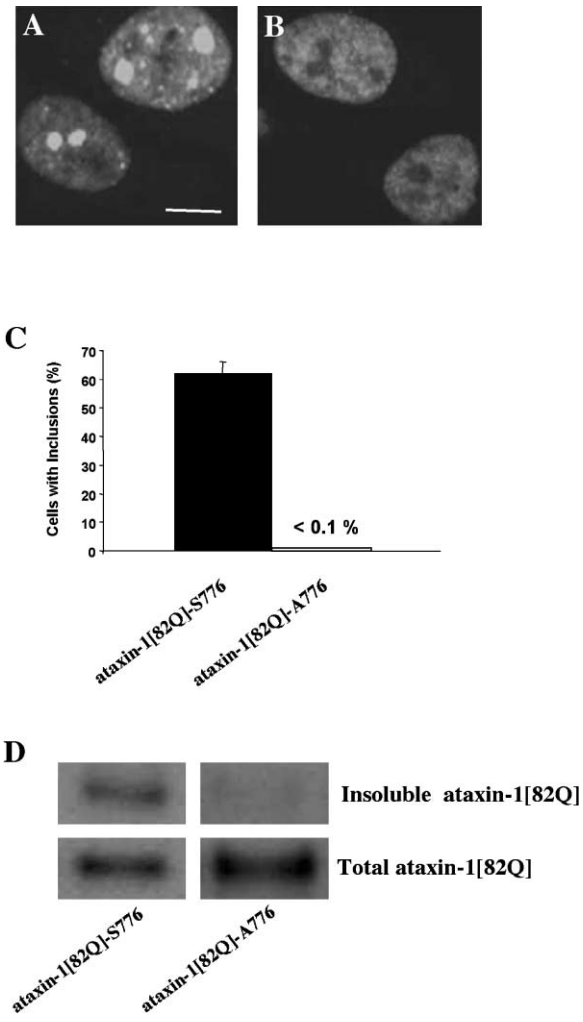

Figure 2. Serine 776 of Ataxin-1 Has a Role in the Formation of Nuclear Inclusions and Solubility of Ataxin-1[82Q] in Transfected Tissue Culture Cells

Ataxin-1 distribution was assessed by immunofluorescence using the ataxin-1 antibody 11750.

(A) Presence of ataxin-1 nuclear inclusions in CHO cells expressing ataxin-1[82Q]-S776. Scale bar equals 5 μm.

(B) Absence of nuclear inclusions in CHO cells expressing ataxin-1[82Q]-A776.

(C) Percent of ataxin-1[82Q]-S776- or ataxin-1[82Q]-A776-expressing cells containing one or more nuclear inclusions.

(D) Western blot with antibody 11750 (Servadio et al., 1995) showing the proportion of ataxin-1[82Q] found in the insoluble fraction versus total ataxin-1 in CHO cells expressing ataxin-1[82Q]-S776 and ataxin-1[82Q]-A776. The amount of insoluble ataxin-1[82Q] decreased from 5% of total to 0.5%, respectively.

expressing ataxin-1[82Q]-S776 to 0.5% in cells expressing ataxin-1[82Q]-A776 (Figures 2D). The finding of trace amounts of ataxin-1[82Q]-A776 in the insoluble fraction argues that it has undergone a conformational change and/or its protein-protein interactions are affected, resulting in less accumulation into inclusions.

Immunolocalization of Phospho-S776 in *SCA1* Transgenic Mice

To examine phospho-S776 ataxin-1 in vivo, we generated an antibody specific for the phospho-S776 form of ataxin-1. Figure 3A depicts the immunization and subsequent purification scheme utilized to obtain the antibody designated PN1168. The specificity of PN1168 was verified by Western blot analyses. Reactivity of PN1168 to ataxin-1 decreased dramatically upon replacing S776 with an Ala (Figure 3B), and thus this antibody requires the presence of a Ser at position 776 for it to react with ataxin-1. Recognition of ataxin-1 by PN1168 was not affected by replacing the Ser at 780 with an Ala or by substituting a Thr for the Lys at position 772 (Figure 3B). However, the recognition of ataxin-1-S776 by PN1168 was decreased substantially by the pretreatment of immune-purified ataxin-1 with phosphatase (Figure 3C). These results show that PN1168 is specific for a phospho-Ser at position 776 of ataxin-1.

Immunohistochemical analyses of cerebellar sections from *SCA1* transgenic mice were used to assess the subcellular localization of S776-phosphorylated ataxin-1 in vivo. In both ataxin-1[30Q] and ataxin-1[82Q] transgenic mice, Purkinje cell nuclei showed the strongest pattern of staining for ataxin-1 with the 11750 antibody. In these mice, ataxin-1 was also readily detected with the 11750 antibody in the cell bodies and throughout the dendrites of the Purkinje cells (Figures 4A and 4C). Reactivity with the phospho-specific antibody PN1168 was also most abundant in the nuclei of Purkinje cells in both ataxin-1[30Q] and ataxin-1[82Q] transgenic mice and detectable to a much lesser extent in Purkinje cell bodies (Figures 4B and 4D). Interestingly, the Purkinje cell dendrites showed no reactivity with the PN1168 antibody. Cerebellar sections from *SCA1* mice expressing ataxin-1[82Q]-T772 in which the NLS was mutated (K772T) were also examined. In this instance, ataxin-1[82Q]-T772 localized predominantly to the cytoplasm of the cell body and throughout the dendritic tree but was minimally reactive with the phospho-S776-ataxin-1 antibody (Figures 4E and 4F). Endogenous murine ataxin-1 was visible in the Purkinje cell nuclei, cell bodies, and dendrites with the 11750 antibody. However, endogenous ataxin-1 failed to stain with PN1168 (Figures 4G and 4H) above the background level seen in cerebellar sections from a *Sca1* knockout mouse (Figures 4I and 4J).

Given that nuclear inclusions of mutant ataxin-1 are a pathological hallmark of SCA1, we examined whether ataxin-1[82Q] in nuclear inclusions was reactive with the phospho-S776-ataxin-1 antibody PN1168. To increase the likelihood of detection, mice homozygous for the B05 transgene were examined. At 4 weeks of age, nuclear inclusions were readily detected in Purkinje cells of $B05^{(tg/tg)}$ mice using the ataxin-1 antibody 11NQ and an anti-ubiquitin antibody (Figures 5A and 5B). These inclusions also stained with the phospho-S776-ataxin-1 antibody (Figure 5C). At this age, the mice begin to develop dendritic abnormalities and have molecular changes based on gene expression study (Clark et al., 1997; Lin et al., 2000). However, at 18 weeks of age, while the nuclear inclusions were large and stained robustly with the ataxin-1 antibody 11NQ and an anti-ubiquitin antibody (Figures 5A and 5B), they were not reactive with the PN1168 antibody (Figure 5C). Thus, with increasing age, nuclear inclusions of ataxin-1[82Q] lost their ability to be stained by the phospho-S776-

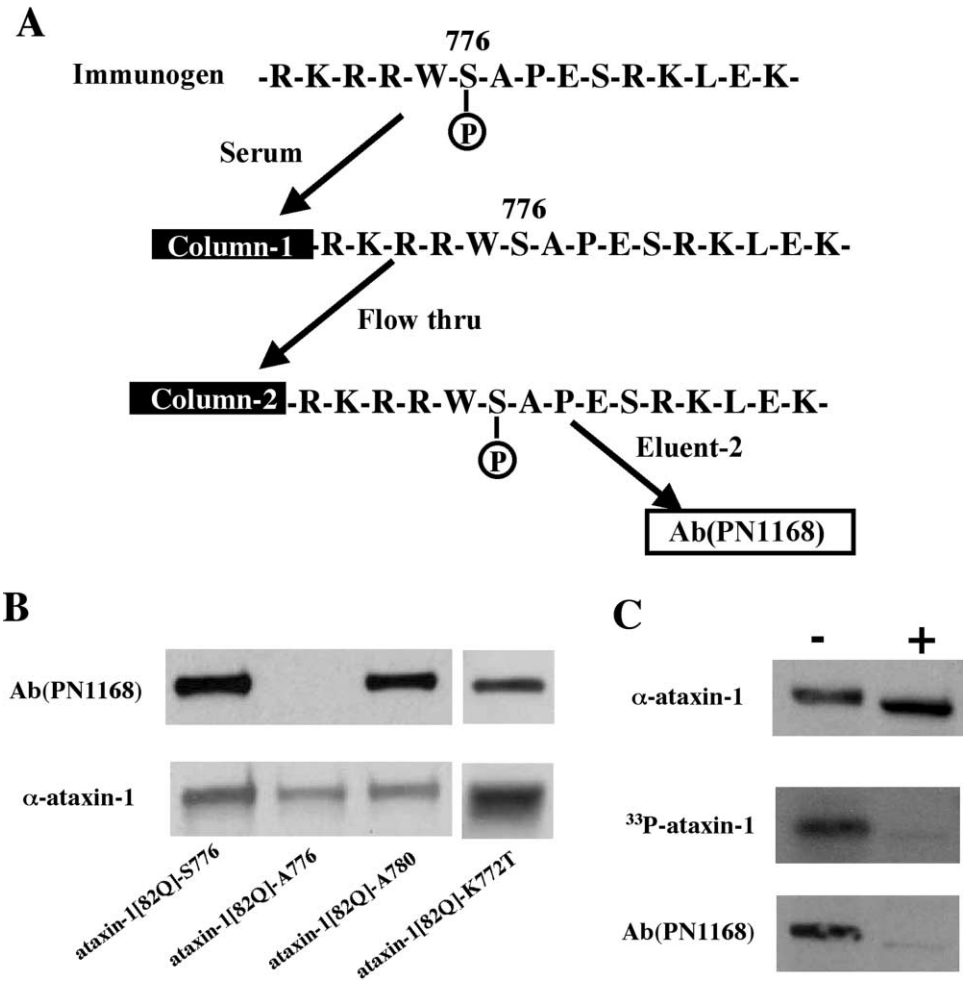

Figure 3. Generation and Specificity of the Phospho-S776-Ataxin-1 Antibody PN1168

(A) The phospho-S776 ataxin-1 peptide used as the immunogen and strategy by which the antibody PN1168 was column purified from serum. Serum was first passed over a column to which the unphosphorylated version of the immunogen peptide has been attached. The flowthrough from this column was subsequently passed over a second column containing the phosphorylated version of the immunogen. Antibodies that bound to the second column were eluted and designated PN1168.

(B) Western blot analyses of ataxin-1-S776, -A776, -T772, and -A780 expressed in transiently transfected COS1 cells. Upper panel is a Western blot with PN1168, demonstrating that this antibody reacts with ataxin-1-S776, -T772, and -A780 but not with ataxin-1-A776. The lower panel is a Western blot using the ataxin-1 antibody 11750, showing the level of ataxin-1 expression in each of the transfected cell populations.

(C) Treatment of immune-purified ataxin-1[82Q] with phosphatase dramatically reduces the amount of ataxin-1 detected with the phospho-S776-ataxin-1 antibody PN1168 and the amount of ^{33}P-ataxin-1 detected by autoradiography. In contrast, phosphatase treatment has no effect on the amount of ataxin-1 detected with ataxin-1 antibody 11750.

ataxin-1 antibody, possibly due to dephosphorylation or masking of epitope by other proteins in the inclusions.

Generation of Ataxin-1[82Q]-A776 Transgenic Mice and Expression of Ataxin-1[82Q]-A776

A *Pcp2*-driven ataxin-1[82Q]-A776 transgene (Figure 6A) was constructed and used to establish transgenic mice as previously described (Burright et al., 1995). Eight ataxin-1[82Q]-A776 founders were obtained. Three lines (designated A776-1, A776-6, and A776-8) demonstrated uniform and high levels of transgene expression in Purkinje cells throughout the cerebellar cortex and therefore were selected for further characterization. Importantly, Northern blot analysis revealed that each of these lines expressed transgene RNA at a level comparable to that seen in ataxin-1[82Q]-S776 mice from line B05$^{(tg/+)}$ (Figure 6B). Results from two of these lines, A776-1 and A776-8, are described in detail.

Expression of the ataxin-1[82Q]-A776 protein was assessed by immunofluorescence using the ataxin-1 antibody 11750 under conditions in which the endogenous murine ataxin-1 was not detected (Skinner et al., 1997). In 5-week-old tg/+ mice, ataxin-1[82Q]-A776-8 was expressed widely in Purkinje cells (Figure 6C) in a fashion similar to that seen in age-matched ataxin-1[82Q]-S776$^{(tg/+)}$ mice from the B05 line (Figure 6D). Examination of immunostained cerebellar sections at high power revealed that ataxin-1[82Q]-A776-8 localized to the nuclei of Purkinje cells (Figure 6E). However, in contrast to the widespread presence of nuclear inclusions containing

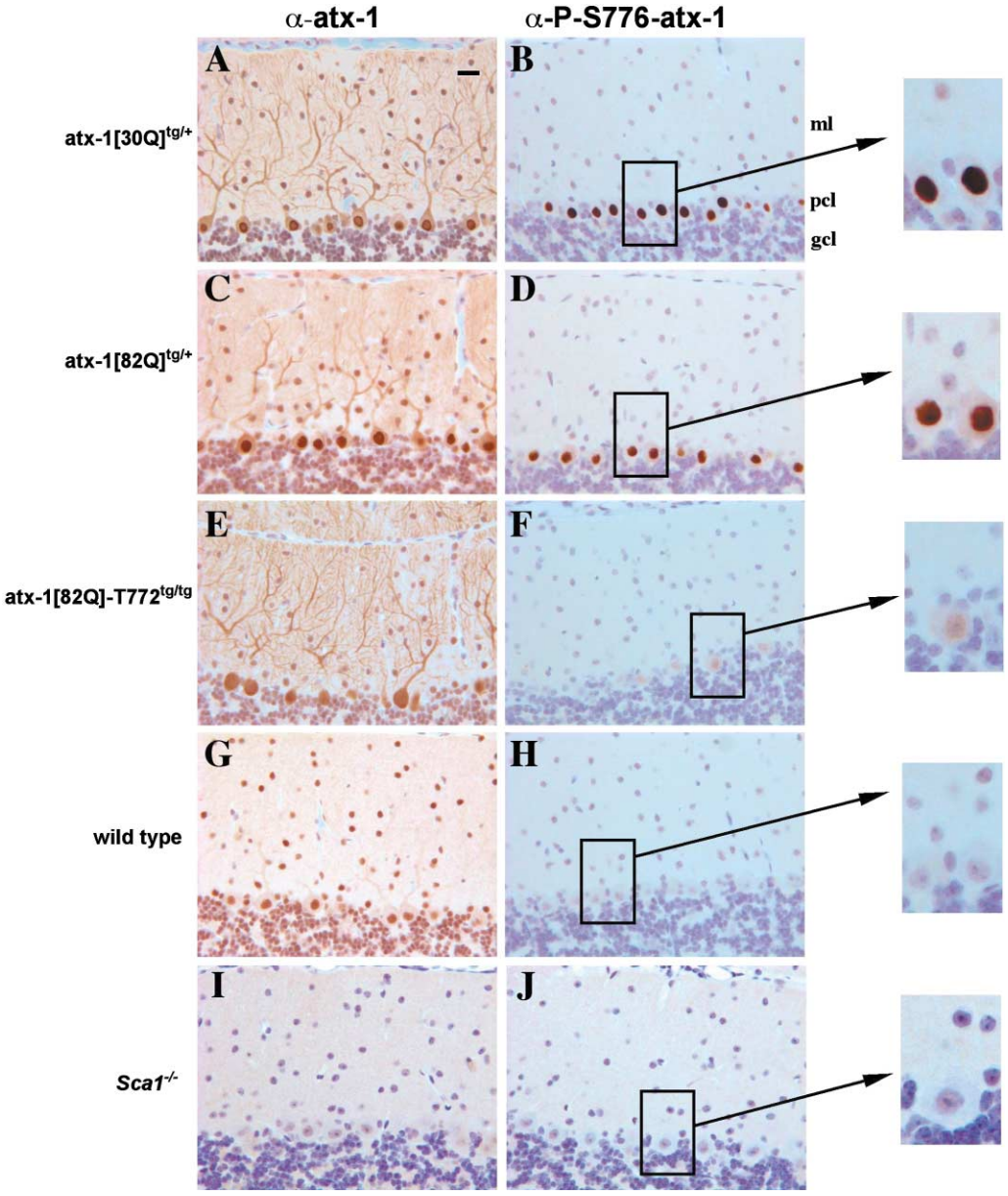

Figure 4. Phospho-S776-Ataxin-1 Localizes to the Nucleus of Purkinje Cells in *SCA1* Transgenic Mice

Total ataxin-1 was detected using antibody 11750 (Servadio et al., 1995) and phospho-S776-ataxin-1 was visualized using antibody PN1168. The outer molecular layer is indicated by ml, the Purkinje cell body layer by pcl, and the inner granule cell layer by gcl.

(A) The ataxin-1-specific antibody 11750 stains ataxin-1[30Q] throughout the Purkinje cells of A02$^{(tg/+)}$ mice. Scale bar equals 30 μm.

(B) The phospho-S776-ataxin-1-specific antibody PN1168 stains nuclear ataxin-1[30Q] in Purkinje cells of A02$^{(tg/+)}$ mice.

(C) The ataxin-1-specific antibody 11750 stains ataxin-1[82Q] throughout the Purkinje cells of B05$^{(tg/+)}$ mice.

(D) The phospho-S776-ataxin-1-specific antibody PN1168 stains nuclear ataxin-1[82Q] in Purkinje cells of B05$^{(tg/+)}$ mice.

(E) The ataxin-1-specific antibody 11750 stains dendritic and cytoplasmic ataxin-1[82Q] in Purkinje cells of K772T$^{(tg/+)}$ mice.

(F) The phospho-S776-ataxin-1-specific antibody PN1168 does not stain dendritic ataxin-1[82Q] in Purkinje cells of K772T$^{(tg/+)}$ mice.

(G) The ataxin-1-specific antibody 11750 stains nuclear endogenous murine ataxin-1 in Purkinje cells of nontransgenic mice.

(H) The phospho-S776-ataxin-1-specific antibody PN1168 does not stain endogenous murine ataxin-1 in Purkinje cells of nontransgenic mice.

(I) The ataxin-1-specific antibody 11750 does not stain Purkinje cells of *Sca1*$^{-/-}$ mice.

(J) The phospho-S776-ataxin-1-specific antibody PN1168 does not stain Purkinje cells of *Sca1*$^{-/-}$ mice.

ataxin-1[82Q]-S776 in 5-week-old B05$^{(tg/tg)}$ animals (Figure 6F), no nuclear inclusions were detectable in Purkinje cells from 5-week-old ataxin-1[82Q]-A776-8$^{(tg/tg)}$ mice (Figure 6E).

To more fully characterize the ability of ataxin-1[82Q]-A776 to form inclusions, we examined Purkinje cells from ataxin-1[82Q]-A776$^{(tg/+)}$ mice for deposition of the ataxin-1[82Q]-A776 at 18, 27, 37, and 46 weeks of age. We determined the percentage of Purkinje cells containing inclusions immunoreactive with the ataxin-1

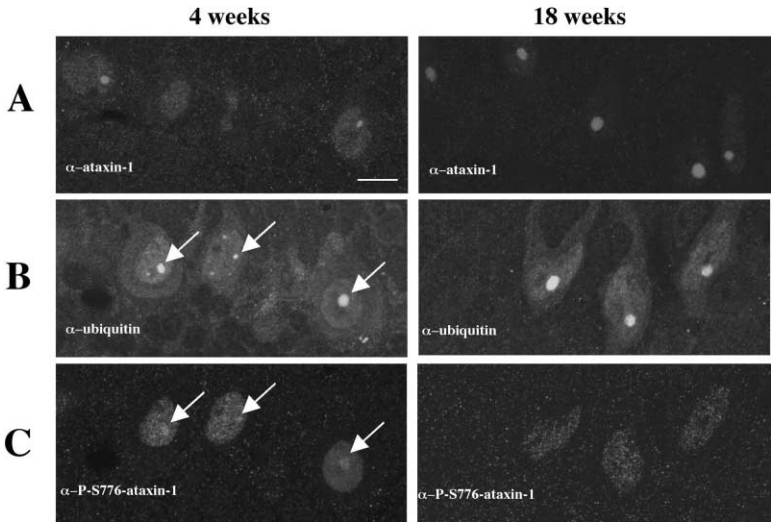

Figure 5. Detection of Phospho-S776-Ataxin-1[82Q] in Nuclear Inclusions Decreases with Age

Homozygous B05 mice were compared at 4 and 18 weeks of age.

(A) The ataxin-1 antibody 11NQ (Skinner et al., 1997) stains nuclear inclusions at 4 and 18 weeks of age in B05$^{(tg/tg)}$ mice. Scale bar equals 10 μm.

(B) Ataxin-1 nuclear inclusions in 4- and 18-week-old B05$^{(tg/tg)}$ mice react with an anti-ubiquitin antibody.

(C) The phospho-S776-ataxin-1-specific antibody PN1168 stains nuclear inclusions at 4 weeks of age but not at 18 weeks of age in B05$^{(tg/tg)}$ mice.

11NQ antibody at the primary fissure of each cerebellum tested (Figure 6G). Inclusions were detectable in 0.2% of the Purkinje cells of 18-week-old ataxin-1[82Q]-A776$^{(tg/+)}$ mice, while in 27-week-old mice, the number of Purkinje cells with inclusions increased to 7%. In 37-week-old ataxin-1[82Q]-A776$^{(tg/+)}$ mice, 18% of the Purkinje cells analyzed had nuclear inclusions of ataxin-1. In 46-week-old mice, this number was similar: 12% of the Purkinje cells contained inclusions. The percent of Purkinje cells with inclusions slowly increased with age, as in the 56-week-old founder animal, 32% of the cells contained inclusions (data not shown). In a 32-week-old homozygous ataxin-1[82Q]-A776 mouse, 16% of the Purkinje cells contained detectable inclusions (data not shown). In contrast, 50% of B05$^{(tg/+)}$ Purkinje cells in 18-week-old mice were found to have ataxin-1 nuclear inclusions, while 100% of the Purkinje cells in 27- and 37-week-old B05$^{(tg/+)}$ mice contained inclusions (Figure 6G). Thus, replacing the Ser with an Ala at position 776 in ataxin-1[82Q] substantially reduced the rate at which nuclear inclusions were formed, in vivo, in *SCA1* transgenic Purkinje cells.

Neurological Phenotype and Neuropathology of Ataxin-1[82Q]-A776 Mice

At all ages examined, the ataxin-1[82Q]-A776$^{(tg/+)}$ mice were indistinguishable from their wild-type littermates in home cage behavior. So far, the ataxin-1[82Q]-A776 hemizygous mice have been evaluated up to 1 year of age. This is an age well past the age of 12 weeks when B05 hemizygous mice show signs of ataxia in home cage behavior (Clark et al., 1997). To insure that the lack of phenotype in ataxin-1[82Q]-A776 mice is not due to slightly lower ataxin-1 levels compared to the B05 mice, we bred the A776 transgenics to homozygosity. These A776$^{(tg/tg)}$ mice, which express at least 25% more transgene RNA than the B05$^{(tg/+)}$ animals, have been carried out to 36 weeks of age and, like the ataxin-1[82Q]-A776 hemizygous mice, the A776 homozygous animals showed no signs of ataxia by home cage behavior.

To uncover subtle coordination deficits that could be missed by looking for ataxic gait in the home cage behaviors, we tested the mice on an accelerating rotarod, a sensitive assay for ataxia. Hemizygous ataxin-1[82Q]-S776 B05 mice show a deficit in rotarod performance as early as 5 weeks of age (Clark et al., 1997). Figure 7A shows that at 19 weeks of age, the impairment in rotarod performance of B05$^{(tg/+)}$ mice was quite severe. In contrast, 19-week-old ataxin-1[82Q]-A776-1 hemizygous mice showed no deficit on the accelerating rotarod and were similar to nontransgenic FVB mice in their performance. We also tested A776-8 hemizygous mice between 43 and 46 weeks of age (Figure 7B). These A776-8 mice showed no deficit compared to 1-year-old nontransgenic FVB mice.

Similarly, cerebellar sections from ataxin-1[82Q]-A776-1$^{(tg/+)}$, ataxin-1[82Q]-A776-8$^{(tg/+)}$, and ataxin-1[82Q]-S776$^{(tg/+)}$ B05 mice were examined at 18, 27, and 37 weeks of age (Figure 7C). By calbindin immunofluorescence, Purkinje cell morphology in 18-week-old ataxin-1[82Q]-A776$^{(tg/+)}$ mice was identical to that of wild-type mice, showing no signs of dendritic thinning or Purkinje cell heterotopia. Importantly, at this age the B05 hemizygous mice showed marked Purkinje cell pathology including considerable dendritic atrophy and several heterotopic Purkinje cell bodies. Similarly, at 27 weeks of age, the morphology of Purkinje cells in the A776$^{(tg/+)}$ mice was unremarkable. This was in stark contrast to the severe atrophy of the Purkinje cell dendrites and disruption of the Purkinje cell layer seen in a 27-week-old B05$^{(tg/+)}$ mouse.

By 37 weeks of age, some sign of dendritic atrophy was apparent in the ataxin-1[82Q]-A776$^{(tg/+)}$ mice (Figure 7C). The thickness of the molecular layer was reduced by 30% compared to wild-type mice. However, in the 37-week-old ataxin-1[82Q]-A776 hemizygous mice, the organization of the Purkinje cell body layer remained intact and no signs of Purkinje cell loss were detected. Similarly, in a 46-week-old A776-8$^{(tg/+)}$ mouse, the Purkinje cell body layer remained intact with only modest thinning of the molecular layer. In contrast, Purkinje cell pathology was very severe in 37-week-old B05$^{(tg/+)}$ mice. Atrophy of the dendritic tree was essentially complete and disorganization of the Purkinje cell layer was extensive. At 32 weeks of age, moderate signs of Purkinje

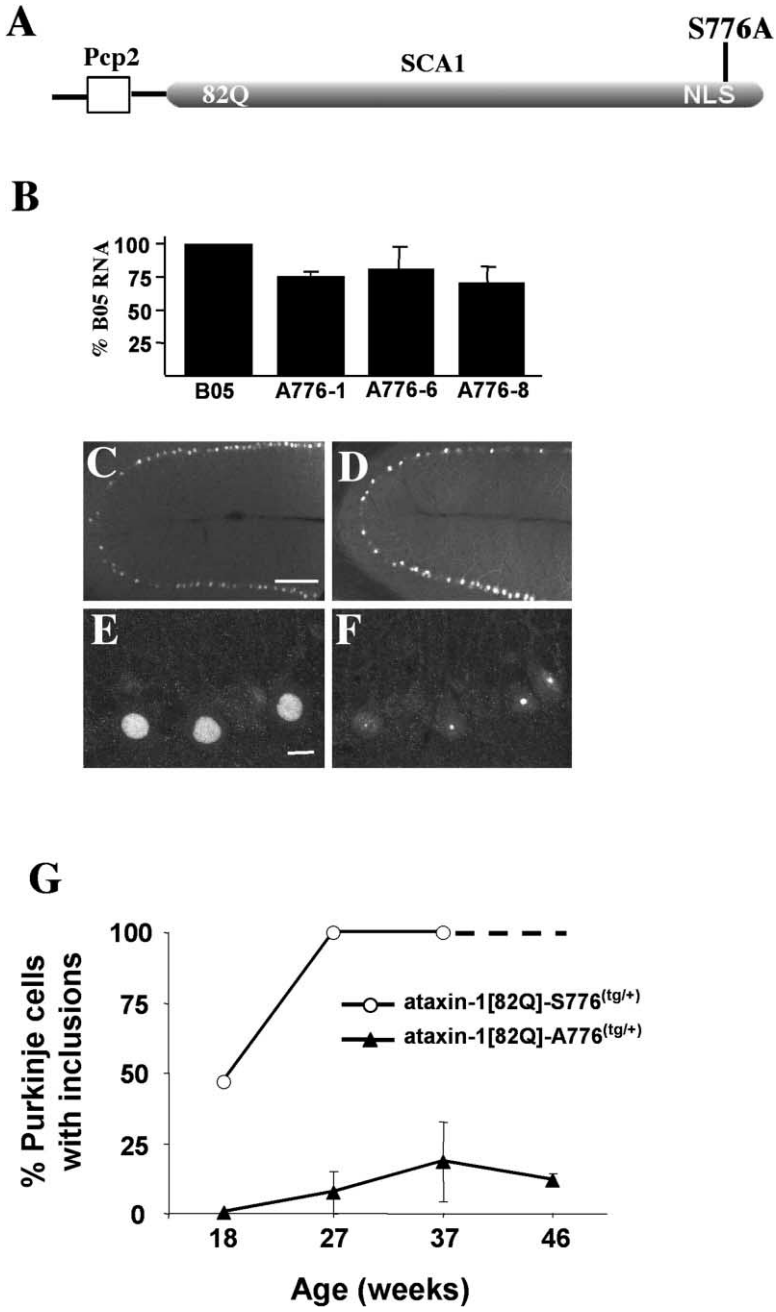

Figure 6. Ataxin-1[82Q]-A776 Localizes to the Nucleus and Has a Reduced Rate of Nuclear Inclusion Formation in Transgenic Mice

(A) Diagram of the *Pcp2*-ataxin-1[82Q]-A776 transgene. Transgene expression was driven by the Purkinje cell-specific *Pcp2* regulatory element.

(B) Relative amount of transgene expression in the three lines of *Pcp2*-ataxin-1[82Q]-A776 transgenic mice. mRNA levels were normalized to the level of transgene mRNA in $B05^{(tg/+)}$ mice.

(C) Expression of ataxin-1[82Q]-A776 in a 5-week-old $A776\text{-}8^{(tg/+)}$ animal. Scale bar equals 100 μm.

(D) Expression of ataxin-1[82Q]-S776 in a 5-week-old $B05^{(tg/+)}$ animal.

(E) Ataxin-1[82Q]-A776 is expressed uniformly throughout the nucleus in Purkinje cells in a 5-week-old $A776\text{-}8^{(tg/tg)}$ animal. Scale bar equals 10 μm.

(F) Ataxin-1[82Q]-S776 forms nuclear inclusions in a 5-week-old $B05^{(tg/tg)}$ mouse.

(G) Comparison of the frequency of nuclear inclusions in transgenic Purkinje cells expressing ataxin-1[82Q]-S776 with the frequency of nuclear inclusions in ataxin-1[82Q]-A776-expressing Purkinje cells. The frequency of nuclear inclusions was determined in $B05^{(tg/+)}$ mice at 18, 27, and 37 weeks of age. For the B05 mice, at 18 weeks, 345 Purkinje cells from two mice were analyzed; at 27 weeks, 272 Purkinje cells from two mice were assessed; and at 37 weeks, 100 Purkinje cells from one mouse were analyzed for the presence of inclusions. The dashed portion of the B05 line indicates that inclusions continue to be in 100% of the Purkinje cells after 37 weeks. The frequency of nuclear inclusions was determined in $A776^{(tg/+)}$ mice (lines 1 and 8) at 18, 27, 37, and 46 weeks of age. The mean and standard error of the mean are given for each time point. At 18 weeks, 438 Purkinje cells from three mice were assessed; at 27 weeks, 387 Purkinje cells from three mice were analyzed; at 37 weeks, 464 cells from three mice were screened; and at 46 weeks, 359 Purkinje cells from three A776 mice were counted for inclusions.

cell pathology were detected in sections examined from an A776 homozygous mouse. Thus, increasing the expression of the A776 transgene to a level above that seen in $B05^{(tg/+)}$ resulted in the appearance of Purkinje cell pathology. However, the severity of pathology in the 32-week-old $A776^{tg/tg}$ mouse was considerably less than that seen in $B05^{tg/+}$ mice at 27 weeks or 18 weeks of age (Clark et al., 1997).

Discussion

Expansion of a glutamine tract is clearly the initiating event in the pathogenesis of polyglutamine neurodegenerative disorders like SCA1. Since the discovery of this mutational mechanism, however, a central issue has been discovering the molecular mediator of toxicity in this class of disease: is it the expanded polyglutamine tract per se, is it the expanded tract within the host protein, or is it the host protein, which becomes particularly toxic due to an altered conformation engendered by the expanded tract?

Studies in cell culture, invertebrate, and mouse models have clearly shown that a polyglutamine peptide is quite toxic to cells and causes progressive phenotypes and cell death. Yet, there is evidence suggesting that host protein sequences, outside of the glutamine tract, impact on the course of disease. A polyglutamine peptide is often much more toxic than one flanked by se-

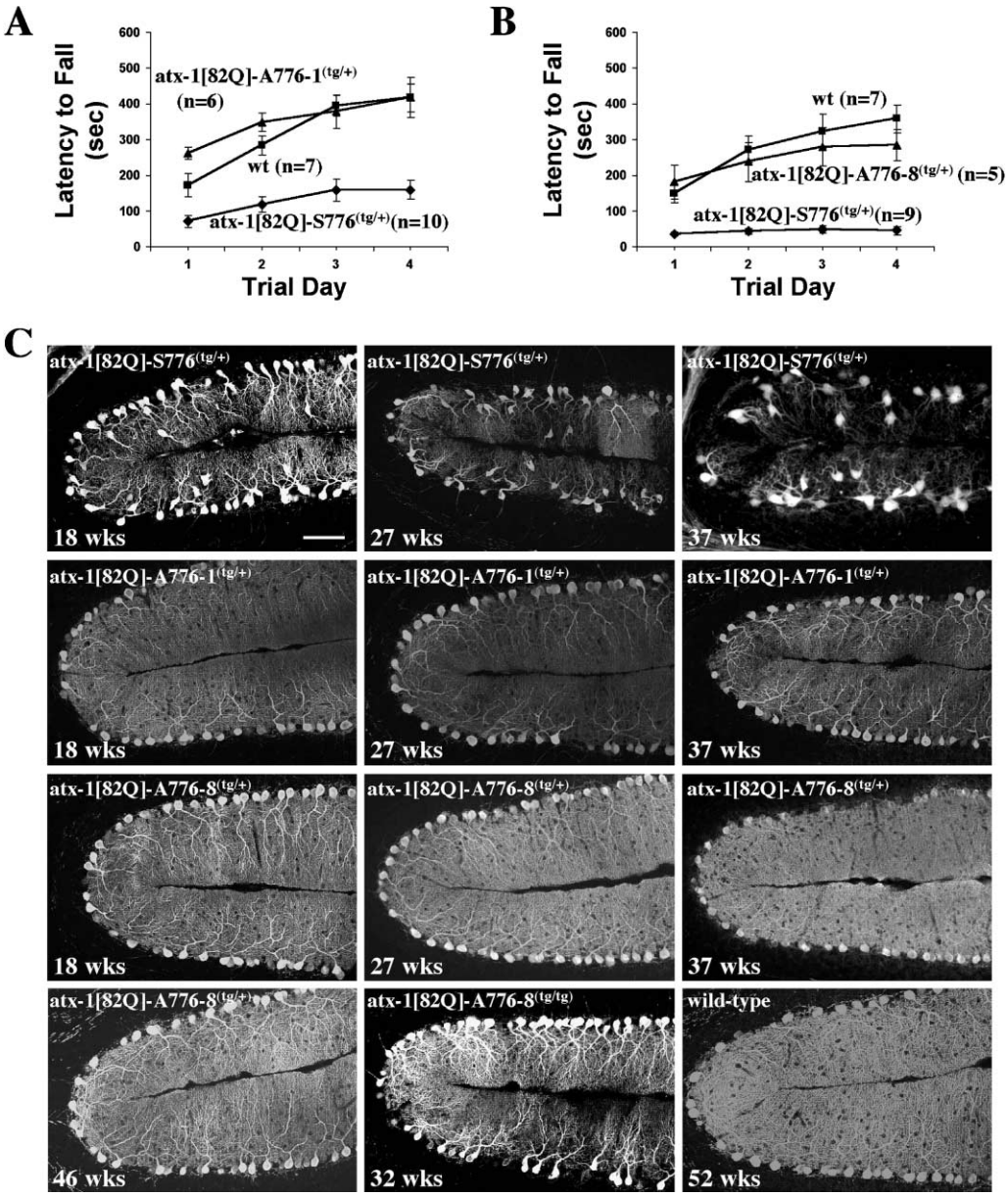

Figure 7. Ataxin-1[82Q]-A776 Is Substantially Less Pathogenic in Transgenic Mice

(A) Rotarod performance of A776-1$^{(tg/+)}$ mice at 19 weeks of age is indistinguishable from nontransgenic littermates and dramatically increased compared to age-matched B05$^{(tg/+)}$ mice (Clark et al., 1997). The mean and standard error of the mean are represented for each trial day for the animals tested.

(B) Rotarod performance of A776-8$^{(tg/+)}$ mice at 43–46 weeks of age is indistinguishable from 1-year-old nontransgenic mice in contrast to the inability of 1-year-old B05$^{(tg/+)}$ mice to perform the task (Clark et al., 1997).

(C) Assessment of Purkinje cell morphology by calbindin immunofluorescence. Mice from two lines expressing ataxin-1[82Q]-A776 (A776-1 and A776-8) or ataxin-1[82Q]-S776 were analyzed between 17 and 37 weeks of age. In addition, a 46-week-old A776-8$^{(tg/+)}$, a 32-week-old A776-8$^{(tg/tg)}$, and a 52-week-old nontransgenic were also analyzed. Scale bar equals 100 μm.

quences from the host protein (Wellington and Hayden, 2000; Zoghbi and Botas, 2002). The importance of the flanking peptide sequence in modulating polyglutamine toxicity is highlighted by data from both human and mouse studies. Each of the polyglutamine disorders is characterized by a specific set of neurological and pathological alterations. For example, in Huntington's disease, jerky body movements, chorea, and psychological changes such as depression are the usual presenting features. Pathologically, HD is characterized by cell loss in the cortex and striatum. In contrast, in SCA1, the presenting clinical features are loss of balance and slurred speech resulting from cerebellar dysfunction and Purkinje cell pathology. In SCA7, retinal dysfunction and visual loss occur in addition to cerebellar disease (Stevanin et al., 2000). Moreover, within the SCAs, there is a dramatic difference in the effect of repeat expansion on disease course. Repeat sizes that lead to late onset

disease in SCA3 cause a juvenile onset disease in SCA1. The findings argue that the expanded repeat tract is not the sole factor that induces pathology and determines disease severity. These findings, however, do not distinguish whether flanking sequence simply modulates the glutamine tract toxicity or whether the host protein itself may become toxic upon glutamine expansion. In this study, we set out to evaluate ataxin-1's phosphorylation in order to gain insight about how such modification may impact pathogenesis.

S776 in Ataxin-1 Is Phosphorylated and Modulates Ataxin-1's Ability to Form Nuclear Inclusions

Using tryptic digestion followed by HPLC and mass spectrometry, we found that ataxin-1 is phosphorylated at serine 776. An antibody, PN1168, generated using an ataxin-1 peptide spanning a phosphorylated serine at position 776, recognized phosphorylated ataxin-1 in vivo, both in transfected cells and transgenic mice.

Immunofluorescence and immunohistochemical studies revealed that by using the phospho-S776-ataxin-1-specific antibody PN1168 both in transgenic mice expressing a wild-type *SCA1* allele (A02$^{(tg/+)}$ mice) and in mice expressing a disease-causing mutant *SCA1* allele (B05$^{(tg/+)}$ animals), S776-phosphorylated ataxin-1 localized primarily to the nucleus. Cytoplasmic ataxin-1 stained much less robustly with the phospho-S776-ataxin-1-specific antibody. The relative decrease in staining with the phospho-S776 antibody compared to total ataxin-1 was particularly noticeable in Purkinje cells of *SCA1* mice expressing ataxin-1[82Q]-T772. In these mice, the NLS of ataxin-1 is mutated and ataxin-1 is localized largely to the cytoplasm of the cell body and throughout the dendritic tree. Interestingly, in COS1 cells transfected with ataxin-1[82Q]-T772, a greater proportion of ataxin-1 localizes to the nucleus than localizes to nuclei of transgenic Purkinje cells (Klement et al., 1998). Thus, the considerable reactivity of ataxin-1[82Q]-T772 with the phospho-S776 antibody PN1168 seen in Western blots of COS1 extracts likely represents nuclear ataxin-1. These data indicate that the phosphorylation of ataxin-1 at S776 is linked to its transport into the nucleus of Purkinje cells.

However, transport of ataxin-1 to the nucleus is not dependent on it being phosphorylated at S776 because an Ala at position 776 did not prevent nuclear localization of full-length ataxin-1[82Q] in cell culture and in Purkinje cells of transgenic mice (see below). Intriguingly, ataxin-1 in the dendritic tree of Purkinje cells, while readily staining with the ataxin-1 antibody 11750, failed to react with the phospho-specific antibody PN1168 (Figure 4), indicating that phosphorylated ataxin-1 at S776 might be excluded from the dendritic tree in Purkinje cells.

An intriguing finding was the pattern of the nuclear deposition of ataxin-1[82Q]-A776. Overexpression of ataxin-1[82Q]-S776 revealed nuclear accumulation of the protein in inclusions (Figure 2A). In contrast, ataxin-1[82Q]-A776 was diffusely distributed in nuclei of transfected cells and was not found in inclusions (Figure 2B). Nuclear inclusion formation in cells transfected with ataxin-1 is typically dependent on length of glutamine tract and integrity of ubiquitin-proteasome degradation pathway (Cummings et al., 1998). Inhibition of the proteasome aggravates the frequency and size of nuclear aggregates and decreases the amount of ataxin-1 in the soluble fraction of protein extracts. Thus, the disappearance of nuclear inclusions may imply better cellular handling of ataxin-1[82Q]-A776. Consistent with this is the fact that we found only 0.5% of ataxin-1[82Q]-A776 in the insoluble fraction of extracts from transfected cells, in contrast to ataxin-1[82Q]-S776, where 5% of the protein was in the insoluble fraction. However, in Purkinje cells, the relationship between ataxin-1[82Q] solubility and inclusion formation is more complex. In Purkinje cells, ataxin-1[82Q]-A776 formed inclusions to a considerably less extent than did ataxin-1[82Q]-S776, yet neither form of ataxin-1[82Q] is detectable by Western blot analysis of cerebellar extracts (Burright et al., 1995, and data not shown).

The Serine at Position 776 Is Critical for Ataxin-1[82Q] Pathogenicity

To test whether our observations in cell culture would also hold in vivo and to determine if the pathogenic effects of ataxin-1[82Q] require a serine at position 776, we generated several lines of transgenic mice that express ataxin-1[82Q]-A776 in cerebellar Purkinje cells. Three lines of mice expressed the transgene at levels comparable to those seen in B05$^{(tg/+)}$ mice that express an allele that encodes for ataxin-1[82Q]-S776. Mice from all three lines did not show any signs of neurological dysfunction as evident by normal rotarod behavior tested at 19 weeks and 43 to 46 weeks and by monitoring their home cage behavior up to 1 year of age. These ages are well beyond the ages at which the B05$^{(tg/+)}$ mice develop an altered neurological phenotype, which usually includes impaired performance on the rotarod at 5 weeks of age and gait ataxia observed in home cages by 12 weeks of age. Thus, having a serine at position 776 is critical for the polyglutamine-induced disease to manifest itself. Lastly, because ataxin-1[82Q]-A776 localized to the nuclei of Purkinje cells, just like the protein with S776, the decrease in toxicity seen with A776 protein cannot be explained by a decrease in its localization in the nucleus. How might a serine at position 776 affect the toxicity of ataxin-1[82Q]?

In the ataxin-1[82Q]-A776 transgenic mice, the protein did not accumulate in nuclear inclusions in a manner similar to what has been observed in the B05 mice. Does this mean that the inclusions are required for disease? We argue that this is not the case. While the presence of protein inclusions is a pathological hallmark of SCA1 and most other polyglutamine diseases (Ross, 1997), the relationship between these entities and disease is complex (Kim and Tanzi, 1998; Sisodia, 1998). At this time it is possible to make several statements about this relationship with a reasonable level of certainty. (1) The ability of mutant ataxin-1 to induce disease in cerebellar Purkinje cells is not dependent on the formation of nuclear inclusions (Klement et al., 1998; Cummings et al., 1999; Watase et al., 2002). (2) The presence of inclusions is exacerbated by interfering with proteasomal degradation and by overexpressing mutant ataxin-1 in cells, mice, and flies (Zoghbi and Botas, 2002). Thus, accumulation of ataxin-1 in nuclear inclusions very likely reflects

that some of this protein is not efficiently degraded and becomes sequestered in these inclusions. (3) Inclusion formation also seems to be dependent on several cellular processes (such as nuclear import, ubiquitination, and protein-protein interaction), and interfering with any of these processes can disrupt inclusion formation. The manner in which such a disruption affects disease is likely dependent on where in the pathway leading to inclusion formation one intercedes. For example, interfering with cellular processes that might sequester the protein in preparation for degradation, e.g., Ube3A (Cummings et al., 1999), would aggravate disease. In contrast, disrupting the ability of ataxin-1 to interact with cellular proteins involved in both inclusion formation and pathogenesis would ameliorate disease, e.g., the A776 substitution described in this study. (4) In a murine knockin model of SCA1 where mutant ataxin-1 is not overexpressed, the increased vulnerability of Purkinje cells that are the last to sequester the protein into inclusions suggest that cellular factors involved in some of the processes aimed at handling the mutant protein may be limiting (Watase et al., 2002).

Studies by Chen and colleagues (2003 [appearing in *Cell*]) demonstrated that S776 is critical for the interaction of ataxin-1 with 14-3-3 and that 14-3-3 enhanced the steady-state levels of ataxin-1[82Q]-S776 in tissue culture cells and in an SCA1 *Drosophila* model. In contrast, 14-3-3 had no effect on the level of ataxin-1[82Q]-A776. These data together with our findings that ataxin-1[82Q]-A776 mice are resistant to polyglutamine-induced pathology point to the critical role of S776 in pathogenesis and to the importance of protein-protein interactions mediated via this serine. Based on the data presented here and on those presented by Chen et al. (2003), we propose that at least two structural features of ataxin-1[82Q] must be in place for disease to develop (Figure 8). Clearly, expansion of the polyglutamine tract to a length within the mutant range must occur. There is considerable data indicating that this expansion results in the misfolding of the protein. We suggest that this effect may cause the protein to be in an alternate or intermediate-folding state that may favor protein-protein interactions and/or somewhat resist degradation. In support of this hypothesis is the finding that overexpression of wild-type ataxin-1 can lead to similar effects, albeit milder, than the protein with an expanded glutamine tract (Fernandez-Funez et al., 2000). This suggests that some wild-type ataxin-1 molecules might take on the alternate folded state favored by the repeat expansion. Second, the surprising new insight from this current study is the finding that, although the N-terminal polyglutamine tract is critical for pathogenesis, it is not sufficient, even when the protein is in the nucleus. Thus, protein/protein interactions in the nucleus that involve only the expanded polyglutamine tract (Waragai et al., 1999; Okazawa et al., 2002) are unlikely to be sufficient for disease. In the case of ataxin-1, molecular events centered on S776 in the C terminus of ataxin-1[82Q] are also critical for pathogenesis.

The finding that ataxin-1[82Q]-A776 forms nuclear inclusions in Purkinje cells at a rate considerably slower that ataxin-1[82Q]-S776 argues that an expanded polyglutamine tract can be efficiently handled by the protein degradation machinery. The dramatic reduction in pathogenicity of ataxin-1[82Q]-A776 in spite of its long glutamine tract highlights the importance of studying the effect of the glutamine expansion in the context of the full-length protein. We showed that S776 is a site of phosphorylation, and Chen et al. (2003) demonstrated that phosphorylation of S776 was required for ataxin-1 to interact with the protein 14-3-3 and that this interaction exacerbated neurodegeneration in a fly model of SCA1. These data demonstrate that host protein sequences outside of the glutamine tract through interactions with a protein like 14-3-3 have a critical role in the accumulation and pathogenicity of a polyglutamine protein. The extent to which the interacting proteins that direct inclusion formation overlap with those that mediate pathogenesis remains to be determined.

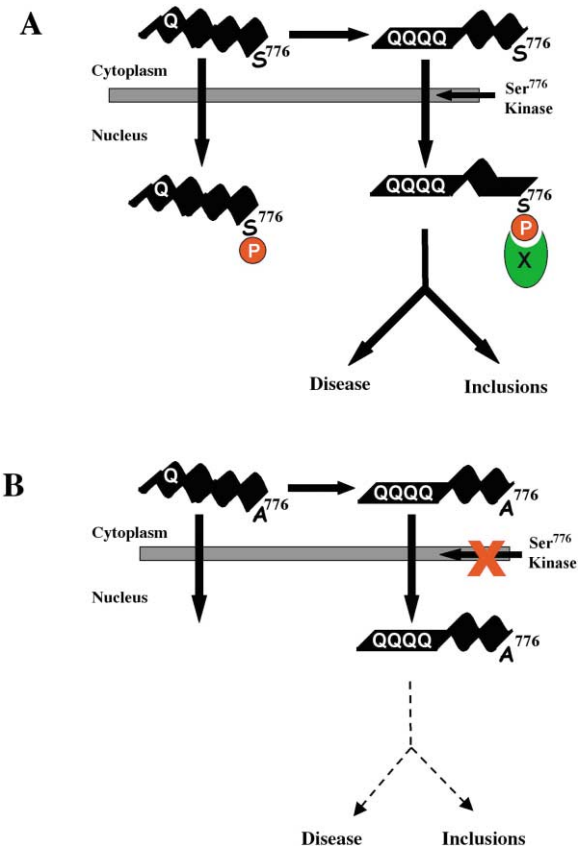

Figure 8. A Model Depicting that Conformation Alterations in Ataxin-1 Caused by the Expanded Polyglutamine Tract as well as Phosphorylation of S776 Are Important for the Development of Disease

(A) Expansion of the polyglutamine tract leads to a conformation change in the protein. This change along with the phosphorylation of serine 776 of ataxin-1 alters the conformation of ataxin-1 that subsequently might affect its interaction with other proteins. These processes are involved in both the formation of inclusions and the development of disease.

(B) Mutation of serine 776 to alanine prevents the phosphorylation of this residue, perhaps blocking phosphorylation and the conformation change induced by this modification of ataxin-1. The result is a dramatic dampening of disease progression and slowing inclusion formation as indicated by the dashed lines.

Experimental Procedures

Constructs

Plasmids for transient transfection experiments were constructed by placing the ataxin-1 cDNA into the eukaryotic expression vector

pCDNA1amp (Skinner et al., 1997). To change the amino acid at position 776, the QuickChange site-directed mutagenesis kit (Stratagene) was utilized. FLAG-tagged pCDNA-ataxin-1[30Q] or pCDNA-ataxin-1[82Q] was used as the PCR template (Skinner et al., 1997). Using a mammalian codon frequency table, we changed the serine codon (UCG) to alanine (GCC). The ataxin-1 A776 transgene was generated by replacing the *Bst*EII-*Nar*I fragment from PS-82 (Burright et al., 1995) with the *Bst*EII-*Nar*I fragment from the pCDNA-ataxin-1-A776-[82Q] mammalian expression vector described above. The sequence and the polyglutamine tract length of all constructs were confirmed by sequencing.

Generation of Cell Lines Stably Expressing Ataxin-1

The *SCA1* cDNAs from pCDNA-ataxin-1[82Q]-S776 and pCDNA-ataxin-1[82Q]-A776 were subcloned into pTRE (Clontech). The pTRE-SCA1 plasmids were cotransfected with pTK-Hyg into the CHO-AA8 Tet-off cell line (Clontech). Stable cell lines were isolated by selection in hygromycin. Hygromycin-resistant clones were recloned and screened for ataxin-1 expression by Western blotting and immunofluorescence.

Mass Spectroscopy Analysis

Ataxin-1[30Q] was immunoprecipitated from stably transfected CHO cells using the ataxin-1 antibody 11NQ (Skinner et al., 1997). Cells (20×10^6) were lysed in 0.25 M Tris-Cl (pH 7.5) containing 1× protease inhibitors (Roche Biochemicals) and phosphatase inhibitor cocktails I and II (Sigma) by three cycles of freeze-thawing. The 11NQ antibody was added to the lysate and was incubated at 4°C with rotation overnight. Immune complexes were collected by incubation for 1 hr with protein G sepharose beads (Amersham Pharmacia Biotech). Following incubation, the complexes were collected by centrifugation at 2500 rpm for 4 min at 4°C and washed four times in RIPA buffer (50 mM Tris-Cl [pH 8.0], 150 mM NaCl, 1% NP40, 0.5% deoxycholate, 0.1% SDS). Beads were resuspended in 2× SDS sample buffer, boiled, and run on a 4%–12% Bis-Tris acrylamide gel (Invitrogen). Following electrophoresis, the gel was stained for 15 min with Coomassie and washed with ultrapure water for 60 min. To quantify the amount of purified protein, the intensity of the ataxin-1 bands were compared with the intensity of the known concentrations (0.1 μg, 0.2 μg, 0.5 μg, and 1 μg) of the 100 kDa band of the BenchMark protein ladder (Invitrogen). Ataxin-1-containing bands that had an intensity of at least 0.1 μg per band were excised and stored at −20°C. We repeated the immunoprecipitation protocol and pooled approximately 50 μg immune-purified ataxin-1. Tryptic digestion and sequence analysis was performed at the Harvard Microchemistry Facility. This analysis consisted of microcapillary reverse-phase HPLC nano-electrospray tandem mass spectrometry on a Finnigan LCQ quadruple ion trap mass spectrometer.

Cell Transfections, Protein Analysis, and Immunofluorescence

COS1 cells growing on 60 mm dishes were transiently transfected using Effectene (Qiagen) as per the manufacturer's recommended protocol. Forty-eight hours posttransfection, cells were washed in PBS and lysed in 0.5 ml lysis buffer (50 mM Tris-Cl [pH 7.5], 2.5 mM $MgCl_2$, 100 mM NaCl, 0.5% Triton X-100, 1× protease inhibitors [Roche Biochemicals], phosphatase inhibitor cocktails I and II [Sigma]). The cells were lysed on the plates by rocking at 4°C on ice for 15 min. The DNA in the lysate was sheared by passing the lysate through a 21-gauge syringe ten times followed by a 25-gauge syringe five times. The lysate was cleared by centrifugation at 14,000 rpm for 10 min at 4°C. The protein concentration was determined using protein assay dye reagent (Bio-Rad). Twenty micrograms of protein was loaded in duplicate wells of a 3%–8% Tris-acetate polyacrylamide gel (Invitrogen) and transferred to nitrocellulose membrane (Protran, Schleicher and Schuell). One membrane was probed with anti-ataxin-1 (11750, 1:5000) and the other with anti-S776 phosphorylated ataxin-1 (PN1168, 1:1000).

The subcellular distribution of ataxin-1 was assessed in stably transfected CHO cells by immunostaining as previously described (Skinner et al., 1997). Cells were plated onto coverslips and stained 48 hr later with either M5 (anti-FLAG, 1:200, Sigma) or with 11750 (anti-ataxin-1, 1:200). To determine the frequency of inclusion formation in tissue culture cells, 200 transfected cells from each experiment were assessed for the presence of inclusions. Lysates from CHO cells growing on 60 mm cell culture plates expressing either S776-ataxin-1[82Q] or A776-ataxin-1[82Q] were used to separate insoluble from soluble ataxin-1. The cells were lysed in 450 μl RIPA buffer (150 mM NaCl, 1% SDS, 1% Triton X-100, 50 mM Tris-Cl [pH 7.5], 100 μg/ml PMSF) for 45 min on ice. DNA in the lysate was sheared as described above. A fraction of the lysate (150 μl) was removed to be used to determine total ataxin-1 expression. The remainder of the lysate was centrifuged at 16,000 × g for 15 min at 4°C and separated into soluble (supernatant) and insoluble (pellet) fractions. Prior to PAGE, the insoluble fraction was solubilized in 300 μl of 1× SDS sample buffer. Western blot analysis was performed and probed with anti-ataxin-1 11750 as described above.

Analysis of Ataxin-1 Phosphorylation in Tissue Culture Cells

Analysis of ataxin-1 phosphorylation was performed in transiently transfected COS1 cells expressing ataxin-1 with either 30 or 82 glutamine repeats. Thirty-six hours posttransfection, the cells were labeled for 7 hr with ^{33}P-orthophosphate (ICN) at a concentration of 750 μCi/ml. Following labeling, the cells were washed two times with PBS and lysed in 0.5 ml lysis buffer (50 mM Tris-Cl [pH 7.5], 2.5 mM $MgCl_2$, 100 mM NaCl, 0.5% Triton X-100, 1× protease inhibitors [Roche Biochemicals], phosphatase inhibitor cocktails I and II [Sigma]). The cells were lysed on the plates by rocking at 4°C on ice for 15 min. The DNA in the lysate was sheared by passing the lysate through a 21-gauge syringe ten times followed by a 25-gauge syringe five times. The lysate was cleared by centrifugation at 14,000 rpm for 10 min at 4°C. Ataxin-1 was immunoprecipitated from the lysate using the ataxin-1 antibody 11750 by incubation with rotation overnight at 4°C. The ataxin-1 immune complexes were captured by the addition of washed protein-G sepharose beads (Amersham Pharmacia Biotech) by incubation with rotation for 4 hr at 4°C. The immune precipitates were collected by centrifugation, washed three times with lysis buffer, and resuspended in 2× SDS sample loading buffer. Boiled samples were loaded onto a 3%–8% Tris-Acetate polyacrylamide gel (Invitrogen). Following electrophoresis, proteins were transferred to a nitrocellulose membrane (Protran, Schleicher and Schuell). The membrane was subjected to autoradiography to determine the amount of ^{33}P incorporation. Following autoradiography, the membrane was subjected to Western blot analysis using the anti-polyglutamine antibody 1C2 (Chemicon) to normalize for the amount of ataxin-1 in each sample. In the case of ataxin-1 with 30 glutamines, we probed the membrane with anti-ataxin-1 11750 (Servadio et al., 1995).

Characterization of an Ataxin-1 S776 Phospho-Specific Antibody (PN1168)

The ataxin-1 S776 phospho-specific antibody was generated and affinity purified by New England Peptide (Fitchburg, MA). Briefly, the S776 phosphorylated peptide (see Figure 3) was used to immunize two rabbits. Serum collected from these rabbits was passed over an affinity column that had the unphosphorylated form of the immunizing peptide bound to the matrix. The flowthrough from this column was passed over a second column that had the phosphorylated immunizing peptide bound to the matrix. The eluent from this column was designated antibody PN1168.

The specificity of PN1168 was assessed by treating immunoprecipitated ataxin-1 with shrimp alkaline phosphatase (USB). COS1 cells were transiently transfected with pCDNA-ataxin-1[82Q] and labeled with ^{33}P-orthophosphate and immunoprecipitated as described above using 500 μl lysis buffer (50 mM Tris-Cl [pH 7.5], 2.5 mM $MgCl_2$, 100 mM NaCl, 0.5% Triton X-100, 1× protease inhibitors [Roche Biochemicals], phosphatase inhibitor cocktails I and II [Sigma]). Following incubation with the protein-G sepharose beads, the immunoprecipitate was washed two times with lysis buffer followed by two washes with phosphatase buffer (20 mM Tris-Cl [pH 8.0], 10 mM $MgCl_2$). The immunoprecipitate was divided into two equal portions; one half was untreated while the other half was treated for 45 min with 14 U of shrimp alkaline phosphatase at 37°C. The untreated sample was also incubated at 37°C. The treated and untreated samples were run in duplicate on a 3%–8% Tris-acetate polyacrylamide gel (Invitrogen). Following electrophoresis and transfer to nitrocellulose membrane (Protran, Schleicher and Schuell), the membrane was subjected to autoradiography. Upon

completion of autoradiography, one replicate was probed with PN1168 (1:1000) while the other was probed with 11750 (1:5000).

Immunohistochemical Staining of Mouse Cerebellum

Immunohistochemical staining of mouse cerebellum was performed as previously described (Klement et al., 1998). Immunohistochemistry was performed on 5 μm microtome sections from paraffin-embedded brains. After rehydration, epitopes were unmasked by steaming for 10 min in pH 6.0 citrate buffer. Staining was carried out using the ABC Elite kit (Vector). The sections were blocked for 20 min in normal serum, incubated overnight at 4°C (11750, 1:10,000 or PN1168, 1:1,000), washed briefly, and incubated for 30 min at room temperature with biotinylated anti-rabbit secondary antibody. The sections were washed briefly, incubated with ABC reagent, washed, exposed for several minutes to DAB substrate, washed, counterstained with hematoxyline, dehydrated in graded alcohols and xylol, and mounted.

Immunofluorescent Staining of Mouse Cerebellum

Immunofluorescent staining of mouse cerebellum was performed as previously described (Skinner et al., 1997). Epitopes were unmasked by boiling three times for 15 s each in 0.01 M urea. The sections were blocked for 1 hr in 2% normal goat serum, 0.3% triton X-100 in PBS. After blocking, the sections were incubated for 48 hr at 4°C in blocking solution containing primary antibody 11750 (1:2000), 11NQ (1:2000), PN1168 (1:500), or calbindin (1:1000). The monoclonal ubiquitin antibody (R&D Systems) was used at a dilution of 1:1000. The sections were washed four times in PBS and incubated for 48 hr in blocking solution containing secondary antibody. Anti-mouse- or anti-rabbit-conjugated Alexa Fluor 488 (Molecular Probes) was used at a dilution of 1:500, and anti-mouse- or anti-rabbit-conjugated Cy3 (Jackson Immunoresearch) was used at a dilution of 1:500. The exception to this is that anti-mouse- or anti-rabbit-conjugated Cy3 was used at a dilution of 1:1000 when the primary antibody was directed against calbindin. Sections were washed as described above and mounted onto microscope slides using glycerol-gelatin (Sigma) supplemented with n-propyl gallate as a preservative. Images were collected on a confocal microscope (Bio-Rad, MRC 1000). In order to compare staining intensities within a given experiment, the collection parameters were held constant.

To determine the frequency of inclusions in SCA1 transgenic mice, we analyzed Purkinje cells from four serial 10 μm sections from the primary fissure of midline sections stained with the ataxin-1 antibody 11NQ. Typically, 25 Purkinje cells per section were analyzed.

Generation and Maintenance of Transgenic Lines

The ataxin-1[82Q]-A776 transgene was linearized with *Sal*I, gel isolated, and purified. The transgene was purified by phenol/chloroform extraction, chloroform extraction, and ethanol precipitation and resuspended in injection buffer (10 mM Tris-Cl [pH 8.0], 0.1 mM EDTA) at a concentration of 4 ng/μl. The Mouse Genetics Laboratory (Univ. of MN) derived potential ataxin-1[82Q]-A776 transgenic founder animals by microinjecting the transgene into FVB/N embryos and implanted them into pseudopregnant females. To identify founder animals, PCR and Southern analysis was performed on tail DNA as previously described (Burright et al., 1995).

Hemizygous sibling matings were performed to generate homozygous *SCA1* transgenic animals. Homozygous animals were identified by Southern blot analysis and confirmed by breeding to FVB/N wild-type mice. Southern blots were probed with a *Pcp2* cDNA in order to compare transgene copy number to endogenous *Pcp2*.

RNA Analysis

For Northern blot analysis, RNA was isolated from one-half of a cerebellum using Trizol reagent (Invitrogen) following the manufacturers recommended protocol. RNA from 5- to 9-week-old animals was eletrophoresed in the presence of glyoxal, blotted to a nylon membrane, and probed with an ataxin-1 cDNA. Blots were subsequently probed with a *GAPDH* cDNA probe to ascertain the amount of RNA loaded per lane. The amount of transgene RNA was normalized to the amount of *GAPDH* RNA in each lane.

Assessment of Motor Ability Using the Rotarod

The accelerating rotarod apparatus was used to assess motor ability as previously described (Clark et al., 1997). The mice were given four trials per day for four consecutive days. On each day between trials, the mice were given a 10 min rest. During a trial the rod accelerated from 4 to 40 rpm over the first 5 min and maintained a speed of 40 rpm for the remainder of the test. The test lasted until the mouse fell from the rod or 10 min had expired, whichever came first. Data from the A776 mice and nontransgenic littermates were compared to historical data from B05 ataxin-1[82Q] animals (Clark et al., 1997). Statistical analyses were performed using a Student's t test.

Acknowledgments

We thank C. Byam and C. Forster for their technical assistance. This work was supported by grants from the National Ataxia Foundation (M.D.K.), the Bob Allison Ataxia Research Center (M.D.K.), and NS22920 (H.T.O. and H.B.C.) and NS27699 (H.Y.Z.) from the NINDS/NIH. H.Y.Z. is an Investigator of the Howard Hughes Medical Institute.

Received: December 17, 2002
Revised: April 7, 2003
Accepted: April 21, 2003
Published: May 7, 2003

References

Banfi, S., Servadio, A., Chung, M.-Y., Kwiatkowski, T.J., Jr., McCall, A.E., Duvick, L.A., Shen, Y., Roth, E.J., Orr, H.T., and Zoghbi, H.Y. (1994). Identification and characterization of the gene causing type 1 spinocerebellar ataxia. Nat. Genet. *7*, 513–519.

Burright, E.N., Clark, H.B., Servadio, A., Matilla, T., Feddersen, R.M., Yunis, W.S., Duvick, L.A., Zoghbi, H.Y., and Orr, H.T. (1995). SCA1 transgenic mice: a model for neurodegeneration caused by an expanded CAG trinucleotide repeat. Cell *82*, 937–948.

Chai, Y., Koppenhafer, S.L., Shoesmith, S.J., Perez, M.K., and Paulson, H.L. (1999). Evidence for proteasome involvement in polyglutamine disease: localization to nuclear inclusions in SCA3/MJD and suppression of polyglutamine aggregation in vitro. Hum. Mol. Genet. *8*, 673–682.

Chen, H.-K., Fernandez-Funez, P., Acevedo, S.F., Lam, Y.C., Kaytor, M.D., Fernandez, M.H., Aitken, A., Skoulakis, E.M.C., Orr, H.T., Botas, J., and Zoghbi, H.Y. (2003). Interaction of Akt-phosphorylated ataxin-1 with 14-3-3 mediates neurodegeneration in spinocerebellar ataxia type 1. Cell *113*, in press. Published online May 9, 2003.

Clark, H.B., Burright, E.N., Yunis, W.S., Larson, S., Wilcox, C., Hartman, B., Matilla, A., Zoghbi, H.Y., and Orr, H.T. (1997). Purkinje cell expression of a mutant allele of SCA1 in transgenic mice leads to disparate effects on motor behaviors, followed by a progressive cerebellar dysfunction and histological alterations. J. Neurosci. *17*, 7385–7395.

Cummings, C.J., Mancini, M.A., Antalffy, B., DeFranco, D.B., Orr, H.T., and Zoghbi, H.Y. (1998). Chaperone suppression of aggregation and altered subcellular proteasome localization imply protein misfolding in SCA1. Nat. Genet. *19*, 148–154.

Cummings, C.J., Reinstein, E., Sun, Y., Antalffy, B., Jiang, Y., Ciechanover, A., Orr, H.T., Beaudet, A.L., and Zoghbi, H.Y. (1999). Mutation of the E6-AP ubiquitin ligase reduces nuclear inclusion frequency while accelerating polyglutamine-induced pathology in SCA1 mice. Neuron *24*, 879–892.

Cummings, C.J., Sun, Y., Opal, P., Antalffy, B., Mestril, R., Orr, H.T., Dillman, W.H., and Zoghbi, H.Y. (2001). Over-expression of inducible HSP70 chaperone suppresses neuropathology and improves motor function in SCA1 mice. Hum. Mol. Genet. *10*, 1511–1518.

Fernandez-Funez, P., Nino-Rosales, M.L., de Gouyon, B., She, W.-C., Luchak, J.M., Martinez, P., Turiegano, E., Benito, J., Capovilla, M., Skinner, P.J., et al. (2000). Identification of genes that modify ataxin-1-induced neurodegeneration. Nature *408*, 101–106.

Genis, D., Matilla, T., Volpini, V., Rossel, J., Davalos, A., Ferrer,

I., Molins, A., and Estivill, X. (1995). Clinical, neuropathologic, and genetic studies of a large spinocerebellar ataxia type 1 (SCA1) kindred: (CAG)n expansion and early premonitory signs and symptoms. Neurology *45*, 24–30.

Hunter, T. (2000). Signaling-2000 and beyond. Cell *100*, 113–127.

Huynh, D.P., Del Bigio, M.R., Ho, D.H., and Pulst, S.M. (1999). Expression of ataxin-2 in brains from normal individuals and patients with Alzheimer's disease and spinocerebellar ataxia 2. Ann. Neurol. *45*, 232–241.

Ishikawa, K., Fujigasaki, H., Saegusa, H., Ohwada, K., Fujita, T., Iwamoto, H., Komatsuzaki, Y., Toru, S., Toriyama, H., Watanabe, M., et al. (1999). Abundant expression and cytoplasmic aggregations of alpha 1A voltage-dependent calcium channel protein associated with neurodegeneration in spinocerebellar ataxia type 6. Hum. Mol. Genet. *8*, 1185–1193.

Kennedy, W.R., Alter, M., and Sung, J.H. (1968). Progressive proximal spinal and bulbar muscular atrophy of late onset: a sex-linked recessive trait. Neurology *18*, 671–680.

Kim, T.-W., and Tanzi, R.E. (1998). Neuronal intranuclear inclusions in polyglutamine disease: nuclear weapons or nuclear fallout? Neuron *21*, 657–659.

Klement, I.A., Skinner, P.J., Kaytor, M.D., Yi, H., Hersch, S.M., Clark, H.B., Zoghbi, H.Y., and Orr, H.T. (1998). Ataxin-1 nuclear localization and aggregation: role in polyglutamine-induced disease in SCA1 transgenic mice. Cell *95*, 41–53.

Lin, X., Antalffy, B., Kang, D., Orr, H.T., and Zoghbi, H.Y. (2000). Polyglutamine expansion down-regulates specific neuronal genes before pathologic changes in SCA1. Nat. Neurosci. *3*, 157–163.

Nakamura, K., Jeong, S.-Y., Uchihara, T., Anno, M., Nagashima, K., Nagashima, T., Ikeda, S., Tsuji, S., and Kanazawa, I. (2001). SCA17, a novel autosomal dominant cerebellar ataxia caused by an expanded polyglutamine in TATA-binding protein. Hum. Mol. Genet. *10*, 1441–1448.

Okazawa, H., Rich, T., Chang, A., Lin, X., Waragai, M., Kajikawa, M., Enokido, Y., Komuro, A., Kato, S., Shibata, M., et al. (2002). Interaction between mutant ataxin-1 and PQBP-1 affects transcription and cell death. Neuron *34*, 701–713.

Orr, H.T. (2001). Beyond the Qs in the polyglutamine diseases? Genes Dev. *15*, 925–932.

Robitaille, Y., Schut, L., and Kish, S.J. (1995). Structural and immunocytochemical features of olivopontocerebellar atrophy caused by the spinocerebellar ataxia type 1 (SCA-1) mutation define a unique phenotype. Acta Neuropathol. (Berl.) *90*, 572–581.

Ross, C.A. (1997). Intranuclear neuronal inclusions: a common pathogenic mechanism for glutamine-repeat neurodegenerative diseases? Neuron *10*, 1147–1150.

Servadio, A., Koshy, B., Armstrong, D., Antalffy, B., Orr, H.T., and Zoghbi, H.Y. (1995). Expression analysis of the ataxin-1 protein in tissues from normal and spinocerebellar ataxia type 1 individuals. Nat. Genet. *10*, 94–98.

Sisodia, S.S. (1998). Nuclear inclusions in glutamine repeat disorders: are they pernicious, coincidental, or beneficial? Cell *95*, 1–4.

Skinner, P.J., Koshy, B.T., Cummings, C.J., Klement, I.A., Helin, K., Servadio, A., Zoghbi, H.Y., and Orr, H.T. (1997). Ataxin-1 with an expanded glutamine tract alters nuclear matrix-associated structures. Nature *389*, 971–974.

Stenoien, D.L., Cummings, C.J., Adams, H.P., Mancini, M.G., Patel, K., DeMartino, N., Marcelli, M., Weigel, N.L., and Mancini, M.A. (1999). Polyglutamine-expanded androgen receptors form aggregates that sequester heat shock proteins, proteasome components and SRC-1, and are suppressed by the HDJ-2 chaperone. Hum. Mol. Genet. *8*, 731–741.

Stevanin, G., Durr, A., and Brice, A. (2000). Clinical and molecular advances in autosomal dominant cerebellar ataxias: from genotype to phenotype and physiopathology. Eur. J. Hum. Genet. *8*, 4–18.

Waragai, M., Lammers, C.H., Takeuchi, S., Imafuku, I., Udagawa, Y., Kanazawa, I., Kawabata, M., Mouradian, M.M., and Okazawa, H. (1999). PQBP-1, a novel polyglutamine tract-binding protein, inhibits transcription activation by Brn-2 and affects cell survival. Hum. Mol. Genet. *8*, 977–987.

Watase, K., Weeber, E.J., Xu, B., Anatalffy, B., Yuva-Paylor, L., Hashimoto, K., Kano, M., Atkinson, R., Sun, Y., Armstrong, D.L., et al. (2002). A long CAG repeat in the mouse *Sca1* locus replicates SCA1 features and reveals the impact of protein solubility on selective neurodegeneration. Neuron *34*, 905–919.

Wellington, C.L., and Hayden, M.R. (2000). Caspases and neurodegeneration: on the cutting edge of new therapeutic approaches. Clin. Genet. *57*, 1–10.

Zoghbi, H.Y. (1996). The expanding world of ataxins. Nat. Genet. *14*, 237–238.

Zoghbi, H.Y., and Botas, J. (2002). Mouse and fly models of neurodegeneration. Trends Genet. *18*, 463–471.

Zoghbi, H.Y., and Orr, H.T. (2000). Glutamine repeats and neurodegeneration. Annu. Rev. Neurosci. *23*, 217–247.